

# Engineering Homologous Molecular Organization in 2D and 3D. Cocrystallization of Pyridyl-Substituted Diaminotriazines with Alkanecarboxylic Acids

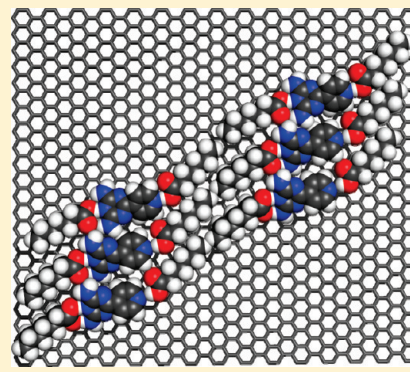
Adam Duong,<sup>†</sup> Marc-André Dubois,<sup>†</sup> Thierry Maris,<sup>†</sup> Valérie Métivaud,<sup>†</sup> Ji-Hyun Yi,<sup>‡</sup> Antonio Nanci,<sup>‡</sup> Alain Rochefort,<sup>§</sup> and James D. Wuest<sup>\*,†</sup>

<sup>†</sup>Département de Chimie and <sup>‡</sup>Faculté de Médecine Dentaire, Université de Montréal, Montréal, Québec H3C 3J7, Canada

<sup>§</sup>Département de Génie Physique, École Polytechnique de Montréal, Montréal, Québec H3A 3A7, Canada

**S** Supporting Information

**ABSTRACT:** Isomeric pyridyl-substituted diaminotriazines **2a–c** and elongated analogue **3** are designed to adopt flattened structures with features that favor adsorption on surfaces and participation in multiple intermolecular interactions. In particular, pyridyl and diaminotriazinyl groups have strong affinities for graphite, and both form coplanar hydrogen-bonded adducts with alkanecarboxylic acids according to reliable motifs. Together, these properties predispose compounds **2a–c** and **3** to be coadsorbed with alkanecarboxylic acids on graphite and to cocrystallize as structures built from hydrogen-bonded sheets. Comparison of the 2D structures of the ordered adlayers (as determined by scanning tunneling microscopy) with the 3D structures of the cocrystals (as determined by X-ray diffraction) showed striking homology, typically with quantitatively similar structural parameters. Together, these results illustrate how a series of related compounds can be engineered to form ordered adlayers and crystalline solids with closely analogous 2D and 3D structures. Specifically, the molecular components should have an affinity for the underlying surface and should engage in coplanar interactions that are strong relative to the energy of adsorption, thereby ensuring that the components are positioned reliably in sheets despite the effect of the surface. In general, compounds with these features should favor similar organization in different states, including monolayers, thin films, and bulk materials, and they promise to be useful in applications requiring behavior that depends predictably on dimensions, such as in thin-film molecular devices.



## INTRODUCTION

The scope of molecular crystal engineering has broadened dramatically in recent years, and its early emphasis on understanding and controlling order in three dimensions (3D)<sup>1</sup> has expanded to encompass a growing interest in the organization of molecules adsorbed on surfaces in two dimensions (2D).<sup>2,3</sup> As a result, the insights of crystal engineers are contributing to advances in all areas of science and technology where molecular organization must be controlled, both in bulk materials and in thin films. Despite the growing utility of crystal engineering, it is still a young field with major unsolved problems. In particular, accurate predictions of the 3D structure of molecular crystals remain notoriously difficult,<sup>4</sup> and the problems are compounded in 2D by the subtle effects of the underlying surface on molecular arrangement. Stiff challenges must therefore be met before molecular organization can be truly mastered in either 2D or 3D.

The challenges of crystal engineering in 2D and 3D are intimately linked. This calls out for an integrated approach in which molecular organization in 3D, determined by X-ray diffraction (XRD) or other methods, is compared systematically with 2D organization on surfaces, as revealed by scanning probe

microscopy (SPM). This integrated approach promises to yield insights unlikely to emerge from studies focused more narrowly on 2D or 3D organization alone. In particular, (1) 3D structures resolved unambiguously by XRD can provide sound models for interpreting images of 2D organization obtained by SPM; (2) SPM can probe fine details of crystallization that cannot readily be examined by XRD, including dynamic phenomena involving individual molecules, structural features at the boundaries of domains, and the nature of defects within domains; and (3) systematic comparison of 2D and 3D structures can clarify the role and relative importance of diverse forces that control molecular organization. Surprisingly, however, there are few reports of integrated analyses of 2D and 3D structures in extended series of related compounds.<sup>5</sup>

Devising compounds that predictably favor similar structures in 2D and 3D is a particularly severe test of our current ability to understand and control molecular organization. When intermolecular

**Received:** February 2, 2011

**Revised:** May 15, 2011

**Published:** June 14, 2011

forces are weak and diffuse, the structuring effect of underlying surfaces may be dominant, and organization in 2D and 3D may show little similarity. However, when intermolecular interactions are strong and directional, they may balance or even outweigh the effect of surfaces and thereby favor closely analogous organization in different states, including monolayers, thin films, and bulk materials. A deeper understanding of this phenomenon is likely to have valuable applications, such as in the design and fabrication of active layers for thin-film molecular devices.

Helpful guidelines have resulted from decades of studying crystallization induced by ordered surfaces, which can lead in favorable cases to epitaxial molecular adsorption in 2D, followed by the layer-by-layer growth of thin films or bulk crystalline phases with similar 3D structures.<sup>6</sup> However, these studies have not provided general prescriptions for devising compounds that crystallize to give predictably homologous 2D and 3D structures, particularly when the underlying surface is not ordered, is not atomically flat, or has lattice parameters that are not well matched with those of 3D crystals of the adsorbate. New tools for ensuring homologous 2D and 3D molecular crystallization are needed.

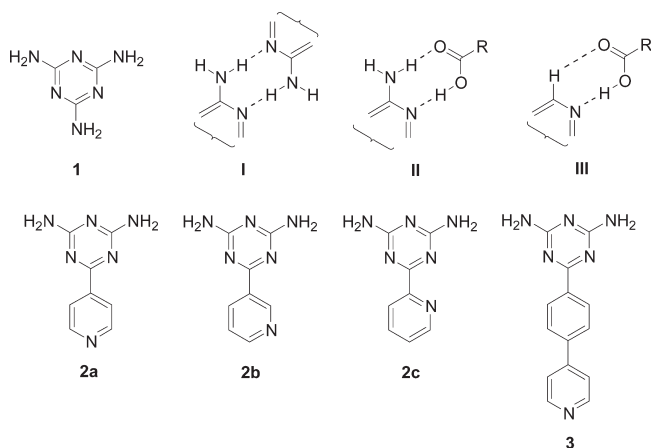
We are exploring an approach based on existing knowledge of epitaxy and related phenomena of surface-induced crystallization, modified by incorporating emerging principles of crystal engineering.<sup>7</sup> Specifically, we have chosen to use compounds with two key properties: (1) the individual compounds have flattened topologies and an inherent affinity for adsorption on surfaces; and (2) the compounds can engage in multiple strong directional interactions in a single plane and can thereby place neighboring molecules in predictable coplanar positions. The goal is to ensure that molecular topology and interactions act in concert to help dictate how crystallization occurs in 2D and 3D, rather than allowing the underlying surface to play a dominant role.

This approach differs from the one followed by many earlier studies of surface-directed crystallization, which have tended to focus on the behavior of relatively simple compounds with weak and nondirectional interactions.<sup>8</sup> In contrast, the use of strong directional coplanar interactions may help make organization more predictably homologous in 2D and 3D, even when true epitaxy is impossible and the underlying surface is not commensurate, atomically flat, or ordered. In addition, previous work has suggested that the ability to engage in well-defined interactions helps prevent molecules from crystallizing in widely different polymorphic forms in 3D,<sup>9</sup> so extensive polymorphism may also be disfavored in 2D. For all these reasons, molecules that engage in strong directional coplanar interactions are potentially valuable components for building predictably homologous 2D and 3D structures.

To facilitate direct structural comparisons, we carried out 2D and 3D crystallizations under conditions as similar as possible. Single crystals were grown from solution without the presence of surfaces except those of the surrounding vessel, and adlayers were deposited from similar or identical solvents, followed by analysis of molecular organization *in situ* at the liquid–solid interface by scanning tunneling microscopy (STM).<sup>10</sup> As the underlying surface, we selected the basal plane of graphite, which adsorbs a wide range of molecules from solution to produce well-defined adlayers.

Recent experimental<sup>11,12</sup> and theoretical<sup>13,14</sup> studies have revealed that melamine (**1**) and related aminotriazines have a strong affinity for graphite. In addition, such compounds associate by

engaging in reliable hydrogen-bonded supramolecular synthons,<sup>15</sup> including homosynthon **I**<sup>9,16–18</sup> and heterosynthon **II** with carboxylic acids.<sup>11,19</sup> The principal atoms involved in both synthons lie in essentially the same plane, ensuring that the planarity of the aminotriazinyl core is extended to a larger assembly. Moreover, pyridyl-substituted aminotriazines **2a–c** are expected to allow further coplanar association with carboxylic acids according to heterosynthon **III**,<sup>20</sup> in which a primary O–H···N hydrogen bond is reinforced by a secondary C–H···O interaction.<sup>21,22</sup> To make the affinity of hydrogen-bonded aggregates of aminotriazines **2a–c** for graphite even greater, we decided to use alkanecarboxylic acids as the hydrogen-bonding partners to take added advantage of the strong adsorption of alkyl chains.<sup>23</sup> In this way, the following factors are expected to act in synergy to favor analogous 2D and 3D assemblies: (1) aminotriazines **2a–c** and alkanecarboxylic acids can adopt flattened conformations and have an inherently high affinity for graphite; (2) they can interact by forming multiple coplanar hydrogen bonds according to reliable patterns **I–III**; and (3) the resulting hydrogen-bonded aggregates can adopt flattened topologies suitable for packing in tapes or sheets. Coassembly is a noteworthy feature of the system we have elected to study because in principle it allows the alkanecarboxylic acid component to be varied without necessarily changing the basic pattern of molecular organization, leading to rational control of metrics in 2D and 3D.



Together, pyridyl-substituted dianaminotriazines **2a–c** and lengthened analogue **3** form a coherent set of compounds with systematic structural alterations. Earlier work has established that triazinyl rings and aryl substituents are normally nearly coplanar.<sup>9,16–18</sup> As a result, compounds **2a–c** and **3** are particularly well designed to form supramolecular aggregates with substantial affinity for graphite, in which a nearly flat aryl-substituted triazinyl core forms hydrogen bonds with multiple coplanar molecules of alkanecarboxylic acid. As described below, we have found that all four compounds **2a–c** and **3** behave as planned, by cocrystallizing with alkanecarboxylic acids to form 2D and 3D structures with striking homology.

## EXPERIMENTAL SECTION

**Syntheses of Pyridyl-Substituted Diaminotriazines **2a–c** and **3**.** Compounds **2a**,<sup>18</sup> **2b**,<sup>24</sup> and **2c**<sup>25</sup> were prepared by methods reported previously. Extended analogue **3** was synthesized in 80% overall yield by the route summarized below, which used Suzuki–Miyaura coupling of 4-bromobenzonitrile

with 4-pyridineboronic acid to make 4-(4-cyanophenyl)pyridine,<sup>26</sup> followed by heating with dicyandiamide according to standard methods.<sup>27</sup> Reagents needed for these syntheses were purchased from commercial sources and used without further purification.

**4-(4-Cyanophenyl)pyridine.**<sup>26</sup> A dried pressure tube was charged with Pd(OAc)<sub>2</sub> (0.030 g, 0.13 mmol), 4-bromobenzonitrile (0.50 g, 2.7 mmol), 4-pyridineboronic acid (0.37 g, 3.0 mmol), and SPhos (0.11 g, 0.27 mmol). Toluene (15 mL), water (5 mL), and methanol (5 mL) were added, and the tube was capped with a septum. The mixture was stirred under N<sub>2</sub> for 10 min at 25 °C, and then K<sub>3</sub>PO<sub>4</sub> (5.8 g, 27 mmol) was added. The septum was replaced with a screw cap, and the mixture was heated at 110 °C until 4-bromobenzonitrile was consumed, as judged by thin-layer chromatography. The mixture was cooled to 25 °C and extracted with dichloromethane. Solvent was removed from the extracts by evaporation under reduced pressure, and the residue was purified by flash chromatography (silica gel, ethyl acetate/hexane 1:4) to give 4-(4-cyanophenyl)pyridine (0.41 g, 2.3 mmol, 85%) as a colorless solid: mp 75–76 °C; IR (ATR) 2917, 2227 cm<sup>-1</sup>; <sup>1</sup>H NMR (400 MHz, CDCl<sub>3</sub>) δ 8.72 (2H, d, <sup>3</sup>J = 5.9 Hz), 7.78 (2H, d, <sup>3</sup>J = 8.2 Hz), 7.73 (2H, d, <sup>3</sup>J = 8.2 Hz), 7.50 (2H, d, <sup>3</sup>J = 5.9 Hz); <sup>13</sup>C NMR (100 MHz, CDCl<sub>3</sub>) δ 151.03, 146.70, 143.00, 133.31, 128.17, 122.01, 118.81, 113.19; HRMS (ESI) calcd for C<sub>12</sub>H<sub>8</sub>N<sub>2</sub> + H m/e 181.0760, found 181.0764.

**2,4-Diamino-6-[4-(pyridinyl)phenyl]-1,3,5-triazine (3).** A mixture of 4-(4-cyanophenyl)pyridine (0.59 g, 3.3 mmol),<sup>26</sup> dicyandiamide (0.55 g, 6.5 mmol), and KOH (0.20 g, 3.6 mmol) in 2-methoxyethanol (30 mL) was heated at reflux for 12 h. The resulting mixture was cooled to 25 °C, the precipitated solid was separated by filtration, and the solid was washed with hot water to give pure 2,4-diamino-6-[4-(pyridinyl)phenyl]-1,3,5-triazine (3; 0.82 g, 3.1 mmol, 94%) as a nearly colorless solid: mp 317 °C; IR (ATR) 3481, 3435, 3399, 3306, 3100, 1647, 1614, 1521, 1436, 1396, 808 cm<sup>-1</sup>; <sup>1</sup>H NMR (400 MHz, DMSO-d<sub>6</sub>) δ 8.67 (2H, d, <sup>3</sup>J = 3.9 Hz), 8.38 (2H, d, <sup>3</sup>J = 7.8 Hz), 7.92 (2H, d, <sup>3</sup>J = 7.8 Hz), 7.78 (2H, d, <sup>3</sup>J = 3.9 Hz), 6.83 (4H, bs); <sup>13</sup>C NMR (100 MHz, DMSO-d<sub>6</sub>) δ 170.46, 168.30, 151.19, 147.19, 140.32, 138.73, 129.31, 127.54, 122.11; HRMS (ESI) calcd for C<sub>14</sub>H<sub>12</sub>N<sub>6</sub> + H m/e 265.1196, found 265.1206. Anal. Calcd for C<sub>14</sub>H<sub>12</sub>N<sub>6</sub>: C, 63.62; H, 4.58; N, 31.80. Found: C, 63.03; H, 4.31; N, 31.65.

**Studies of 2D Crystallization by STM.** All STM experiments were performed at room temperature (20–25 °C) using a JEOL-S200 SPM instrument equipped with a narrow scanner. Platinum/iridium STM tips were mechanically cut from wire (Pt/Ir, 80%/20%, diameter = 0.25 mm). In typical experiments, the freshly cleaved basal surface of HOPG (Structure Probe, Inc., SPI-1 grade) was first imaged to determine the quality of the Pt/Ir tip and the smoothness of the graphite surface. Once this was determined, a droplet (~1 μL) of a saturated solution of pyridydiaminotriazines **2a–c** and **3** in alkanecarboxylic acids was applied. STM investigations were then carried out at the liquid–solid interface in the constant-height mode. STM imaging was performed by changing the tunneling parameters (voltage applied to the tip and the average tunneling current). Raw STM images were processed using a JEOL software package (WinSPM Data Processing System, Version 2.15, R. B. Leane, JEOL Ltd.) and a freeware (WSxM 5.0 Develop 1.2, Nanotec Electrónica S. L.).<sup>28</sup> A smooth 3 × 3 matrix convolution filter was used to produce the final images.

**Semiempirical Modeling of 2D Molecular Organization in Adlayers on Graphite.** Profiles of patterns of contrast in STM images were analyzed to estimate unit cell parameters and to allow initial structural hypotheses to be formulated. Detailed molecular models based on these hypotheses were then calculated, using the semiempirical method RM1.<sup>29</sup> This method is expected to yield models of 2D organization that are qualitatively reliable. However, the method requires only modest computational resources, unlike high-level density-functional approaches in which long-range dispersive interactions are taken into account, such as those we and others have reported earlier.<sup>13,30,31</sup>

Working with either HyperChem Pro 8.0 (PC-based) or HyperChem 4.0 (Intel Mac-based), we first used the Amber force field to minimize the energy of (1) an isolated molecule of each type of adsorbate and (2) a model graphene sheet large enough to accommodate multiple adsorbates. We then allowed an individual molecule of each type of adsorbate to approach the graphene sheet, which was kept fixed to simplify computation. Once the individual molecules had adjusted in response to the underlying surface, as computed using Amber, copies were positioned on the surface according to the initial structural hypothesis. To allow the effect of neighboring adsorbates to be evaluated properly, the number of postulated hydrogen-bonded aggregates placed on the surface was typically large enough to ensure that several were completely surrounded by neighbors. As illustrated in Figures 3, 5, 7, and 9, the number of discrete hydrogen-bonded aggregates ranged from 4 to 8. The energy of the adsorbed assembly was then reminimized using Amber to provide a starting geometry for semiempirical RM1 calculations, which were carried out with either HyperChem or MOPAC2009.<sup>32</sup> These calculations yielded the reported models, in which the assembled molecules have adjusted in response to the presence of their neighbors and an underlying fixed graphene sheet.

This approach to modeling 2D molecular organization on surfaces is attractive for three reasons: (1) it specifically assesses the effect of the underlying surface; (2) it takes neighboring molecules into account; and (3) it can be undertaken with modest computational resources but follows a strategy of analysis related to those used in higher-level DFT approaches.<sup>13,30</sup> Minor shortcomings include the slight aperiodicity seen in Figures 3, 5, 7, and 9, which results from the small finite number of absorbed molecules used in the calculations and the slightly different environments of molecules in the interior and those on the periphery.

**Studies of 3D Crystallization by XRD.** Cocrystals were obtained by slow evaporation of solutions of pyridydiaminotriazines **2a–c** and **3** in alkanecarboxylic acids. Crystallographic data were collected at 150 K using a Bruker Microstar diffractometer with Cu Kα radiation. The structures were solved by direct methods using SHELXS-97, and non-hydrogen atoms were refined anisotropically with SHELXL-97.<sup>33</sup> Hydrogen atoms were treated by first locating them from difference Fourier maps, recalculating their positions using standard values for distances and angles, and then refining them as riding atoms. In all structural studies, calculated powder X-ray diffraction patterns closely matched those obtained experimentally by analysis of bulk crystalline samples, thereby establishing that the samples consisted primarily of a single phase.<sup>34</sup>

**Density-Functional Calculations of Adsorption on Graphene.** Selected examples of adsorption and coadsorption were

**Table 1.** Crystallographic Data for Cocrystals of 2,4-Diamino-6-(4-pyridyl)-1,3,5-triazine (2a), 2,4-Diamino-6-(3-pyridyl)-1,3,5-triazine (2b), and 2,4-Diamino-6-(2-pyridyl)-1,3,5-triazine (2c) with Alkanecarboxylic Acids (C8 = Octanoic Acid and C9 = Nonanoic Acid)

cocrystal	2a·2 C8	2a·2 C9	2b·1 C9	2c·1 C8	2c·1 C9
formula	C <sub>24</sub> H <sub>40</sub> N <sub>6</sub> O <sub>4</sub>	C <sub>26</sub> H <sub>44</sub> N <sub>6</sub> O <sub>4</sub>	C <sub>17</sub> H <sub>26</sub> N <sub>6</sub> O <sub>2</sub>	C <sub>16</sub> H <sub>24</sub> N <sub>6</sub> O <sub>2</sub>	C <sub>17</sub> H <sub>26</sub> N <sub>6</sub> O <sub>2</sub>
crystal system	triclinic	triclinic	triclinic	triclinic	triclinic
space group	P <bar{1}< td=""><td>P<bar{1}< td=""><td>P<bar{1}< td=""><td>P<bar{1}< td=""><td>P<bar{1}< td=""></bar{1}<></td></bar{1}<></td></bar{1}<></td></bar{1}<></td></bar{1}<>	P <bar{1}< td=""><td>P<bar{1}< td=""><td>P<bar{1}< td=""><td>P<bar{1}< td=""></bar{1}<></td></bar{1}<></td></bar{1}<></td></bar{1}<>	P <bar{1}< td=""><td>P<bar{1}< td=""><td>P<bar{1}< td=""></bar{1}<></td></bar{1}<></td></bar{1}<>	P <bar{1}< td=""><td>P<bar{1}< td=""></bar{1}<></td></bar{1}<>	P <bar{1}< td=""></bar{1}<>
<i>a</i> (Å)	4.8615(6)	7.5805(6)	10.3277(19)	8.8653(4)	8.0471(4)
<i>b</i> (Å)	7.4585(9)	11.1838(9)	13.405(2)	9.4282(4)	10.3951(5)
<i>c</i> (Å)	19.034(3)	25.627(2)	13.648(2)	10.7014(5)	11.6890(5)
$\alpha$ (°)	83.881(7)	94.378(4)	92.130(11)	104.685(2)	67.342(2)
$\beta$ (°)	84.671(7)	92.854(4)	106.824(12)	90.861(2)	85.030(2)
$\gamma$ (°)	79.308(7)	101.374(3)	95.855(12)	98.832(3)	89.545(2)
<i>V</i> (Å <sup>3</sup> )	672.44(15)	2119.0(3)	1794.6(5)	853.62(7)	898.59(7)
<i>Z</i>	1	3	4	2	2
$\rho_{\text{calcd}}$ (g cm <sup>-3</sup> )	1.177	1.186	1.282	1.293	1.280
<i>T</i> (K)	150	150	150	150	150
$\mu$ (mm <sup>-1</sup> )	0.660	0.654	0.711	0.726	0.710
<i>R</i> <sub>1</sub> , <i>I</i> > 2σ( <i>I</i> ) (%)	6.32	6.58	8.70	7.01	4.22
<i>R</i> <sub>1</sub> , all data (%)	13.55	14.19	15.84	7.44	4.33
$\omega R$ <sub>2</sub> , <i>I</i> > 2σ( <i>I</i> ) (%)	15.87	16.51	20.91	18.49	11.64
$\omega R$ <sub>2</sub> , all data (%)	19.75	21.41	25.63	19.55	11.77
measured reflections	9662	29039	20766	14242	13101
independent reflections	2369	5617	6368	3105	3214
observed reflections, <i>I</i> > 2σ( <i>I</i> )	1208	2775	3085	2749	3069

modeled by a high-level density-functional approach in which long-range dispersive interactions are taken into account. To allow direct comparison with related studies, we used the same methodology reported in detail in earlier work.<sup>13</sup> Briefly, our calculations were based initially on the local-density approximation (LDA) of density-functional theory (DFT), and they employed a fixed graphene sheet of defined size and geometry (204 atoms of carbon and 40 peripheral atoms of hydrogen). The basis set chosen for atoms of carbon was STO-3G, and 6-31G\* was used for all other atoms. The structures were optimized, and bond dissociation energies of complexes were calculated with respect to the appropriate ground-state species asymptote. In a subsequent step in the calculations, we evaluated the contribution of dispersive interactions, which are not formally taken into account within LDA limits. This was achieved by using the PBE functional to perform single-point calculations on LDA-optimized geometries,<sup>35</sup> in conjunction with semiempirical dispersion corrections (D).<sup>36</sup> The results of such calculations can be described as being at the PBE+D level.

## ■ RESULTS AND DISCUSSION

**3D Cocrystallization of 2,4-Diamino-6-(4-pyridyl)-1,3,5-triazine (2a) with Alkanecarboxylic Acids.** Slow evaporation of a solution of 2,4-diamino-6-(4-pyridyl)-1,3,5-triazine (2a) in octanoic acid at 25 °C yielded cocrystals of composition 2a·2 octanoic acid. The cocrystals proved to belong to the triclinic space group P, and other crystallographic data are summarized in Table 1. Views of the structure are provided in Figure 1. Molecules of compound 2a were found to be statistically disordered (50:50) with respect to a center of inversion.<sup>34</sup> To simplify discussion, structural data for only one orientation are presented.

Each molecule of pyridyl-substituted diaminotriazine 2a forms hydrogen bonds with two molecules of octanoic acid according to well-established supramolecular synthons II and III. The crystallographic data show that full proton transfer does not occur to give the corresponding aminotriazinium or pyridinium carboxylate salts.<sup>37–39</sup> The observed O—H···N(triazine), O···H—N(triazine), and O—H···N(pyridine) distances in synthons II and III have normal values (2.661, 2.938, and 2.611 Å, respectively).<sup>19,20</sup> The secondary C—H···O interaction that normally uses an  $\alpha$  C—H bond of pyridines to help stabilize synthon III has a H···O distance (3.057 Å) longer than the sum of the van der Waals radii. Nevertheless, the carboxyl group is maintained in the plane of the pyridyl ring, and the alkyl chain adopts a fully extended conformation. As expected, the angle formed by the average planes of the triazinyl and pyridyl rings is small (11.1°), resulting in ternary aggregates that are essentially planar. The aggregates then pack to form tapes aligned with the *b* axis (Figure 1a), which are held together by an additional N—H···O hydrogen bond (2.636 Å), augmented by a C—H···O interaction involving an  $\alpha$ -pyridyl C—H bond (H···O distance = 2.874 Å). The hydrogen-bonded tapes then pack to form sheets (Figure 1a), which stack with a slight offset to give the full 3D structure (Figure 1b).

Under similar conditions, cocrystallization of pyridyl-substituted diaminotriazine 2a with nonanoic acid in place of octanoic acid proved to yield a fully analogous structure. The cocrystals were found to belong to the triclinic space group P, and other crystallographic data are presented in Table 1. Views of the structure are shown in Figure 2. Molecules of compound 2a proved to be statistically disordered (50:50) with respect to a center of inversion.<sup>34</sup> For simplification, structural data for only one orientation and one molecule in the asymmetric unit are presented. Again, the observed

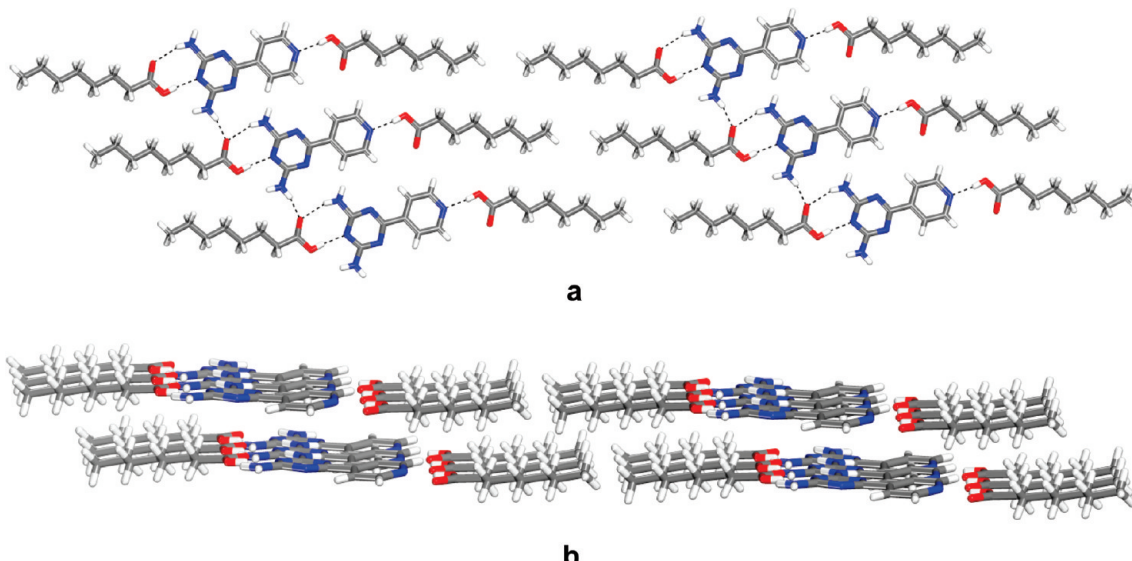


**Figure 1.** Views of the structure of 1:2 cocrystals of 2,4-diamino-6-(4-pyridyl)-1,3,5-triazine (**2a**) with octanoic acid. (a) View of part of a sheet constructed from hydrogen-bonded tapes. Hydrogen bonds are represented by broken lines, and carbon atoms are shown in gray, hydrogen atoms in white, nitrogen atoms in blue, and oxygen atoms in red. (b) View of two stacked sheets.

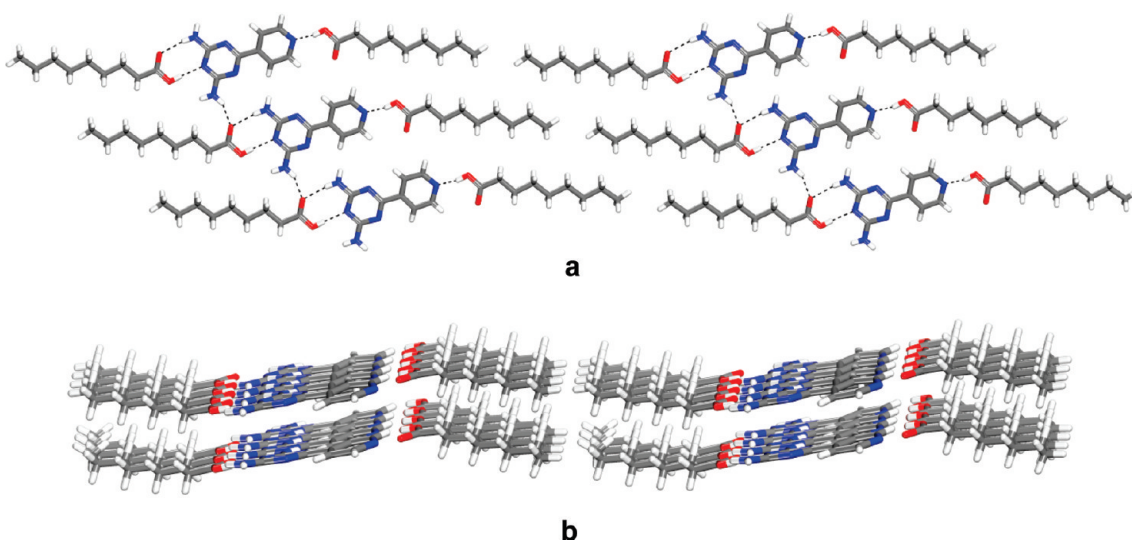


**Figure 2.** Views of the structure of 1:2 cocrystals of 2,4-diamino-6-(4-pyridyl)-1,3,5-triazine (**2a**) with nonanoic acid. (a) View of part of a sheet constructed from hydrogen-bonded tapes. Hydrogen bonds are represented by broken lines, and carbon atoms are shown in gray, hydrogen atoms in white, nitrogen atoms in blue, and oxygen atoms in red. (b) View of two stacked sheets.

O—H $\cdots$ N(triazine), O $\cdots$ H—N(triazine), and O—H $\cdots$ N(pyridine) distances are normal (2.805, 2.936, and 2.481 Å, respectively),<sup>19,20</sup> and synthon III is reinforced as usual by a secondary C—H $\cdots$ O interaction (H $\cdots$ O distance = 2.822 Å). The average angle defined by the planes of the triazinyl and pyridyl rings is characteristically small (9.0°), leading again to nearly planar ternary aggregates that associate to form tapes aligned with the  $\alpha$  axis (Figure 2a). Cohesion of the tapes is ensured in part by an additional N—H $\cdots$ O hydrogen bond (2.710 Å), along with a C—H $\cdots$ O interaction involving an  $\alpha$ -pyridyl C—H bond (H $\cdots$ O distance = 2.776 Å). Packing of the hydrogen-bonded tapes then gives sheets (Figure 2a), which stack to produce the 3D structure (Figure 2b).

**2D Cocrystallization of 2,4-Diamino-6-(4-pyridyl)-1,3,5-triazine (2a) with Alkanecarboxylic Acids.** The observation that both 3D structures consist of hydrogen-bonded sheets with identical 1:2 compositions and closely analogous molecular organization suggests that pyridyl-substituted diaminotriazine **2a** is inherently disposed to coadsorb with alkanecarboxylic acids on graphite to give analogous 2D assemblies. To test this hypothesis, we added a saturated solution of compound **2a** in heptanoic acid to the freshly exposed surface of highly oriented pyrolytic graphite (HOPG), and we analyzed the liquid–solid interface by scanning tunneling microscopy (STM), which revealed an ordered adlayer. A representative image is shown in Figure 3, along with a superimposed unit cell and a model of

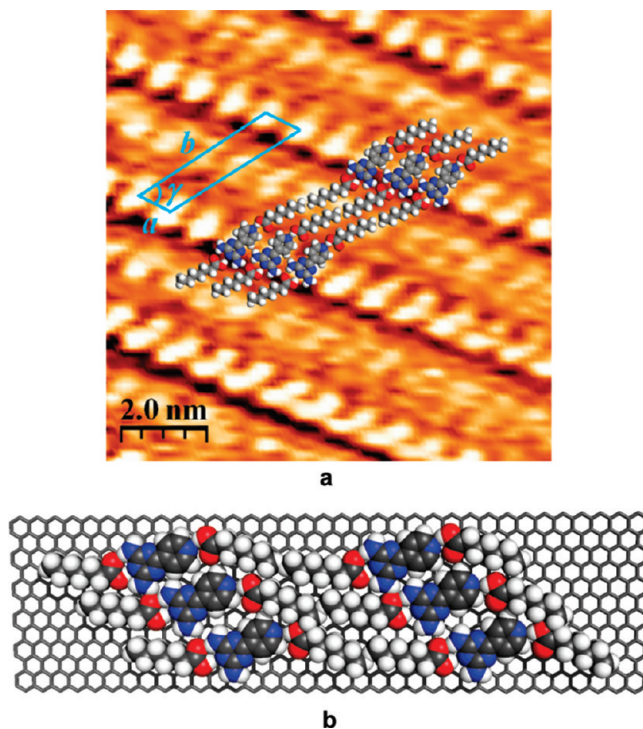


**Figure 3.** (a) STM image of the adsorption of 2,4-diamino-6-(4-pyridyl)-1,3,5-triazine (**2a**) on HOPG (deposition from heptanoic acid, with  $V_{\text{bias}} = -1.51$  V and  $I_{\text{set}} = 0.09$  nA). Superimposed on the image are a scale bar, the measured unit cell, and approximate molecular models added as visual aids to facilitate interpretation of the pattern of contrasts. (b) Detailed semiempirical model of the postulated 2D structure.

the proposed molecular organization, calculated by the semiempirical method described in the Experimental Section.

Examination of the periodic patterns of contrast, combined with analysis of the unit cell parameters ( $a = 7.4$  Å,  $b = 35.1$  Å,  $\gamma = 60^\circ$ ), established that adsorption produces alternating regions of compound **2a** (brighter) and heptanoic acid (darker), which appear to be organized in chiral tapes fully analogous to those observed by XRD (Figures 1a and 2a). These observations suggest that compound **2a** and alkanecarboxylic acids cocrystallize in 2D and 3D in an essentially identical way. This homology is striking because it shows that the components have chosen to form aggregates with the same composition and organization despite potentially disruptive influences such as the effect of the underlying surface.

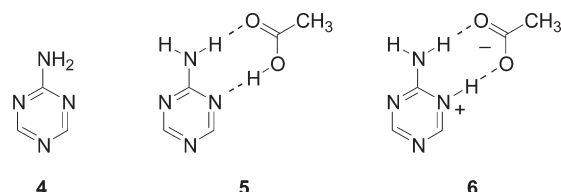
Detailed quantitative analysis of structural parameters in 2D and 3D supports the conclusion that molecular organization is nearly identical. Molecular separation along the tapes in 3D, which is 7.459 Å in cocrystals with octanoic acid and 7.581 Å in cocrystals with nonanoic acid, is virtually the same as that observed in 2D ( $a = 7.4$  Å). In addition, adjacent tapes in 3D cocrystals with octanoic acid are separated by approximately 35.3 Å, as measured along the line defined by the extended alkyl chains, and the value is 37.6 Å in 3D cocrystals with nonanoic acid. Both parameters are consistent with the corresponding distance in 2D cocrystals with heptanoic acid ( $b = 35.1$  Å). Moreover, angles defined by the tapes and alkyl chains in 3D (approximately 47° and 46° in cocrystals with octanoic acid and nonanoic acid, respectively) are similar to the angle observed in 2D ( $\gamma = 60^\circ$ ). We attribute the small differences to slight

**Table 2. Energies of Adsorption of Acetic Acid, 2-Amino-1,3,5-triazine (**4**), and Hydrogen-Bonded Complex **5** on Graphene, as Calculated at the PBE+D Level**

adsorbate	energy of adsorption (kcal/mol)
acetic acid	13.8
2-amino-1,3,5-triazine ( <b>4</b> )	23.1
complex <b>5</b>	28.2

nonplanarity of the sheets observed in 3D and to efforts of the adsorbates to achieve registration with graphite in 2D.

Although the close quantitative similarity of structural parameters in 2D and 3D suggests that the assembled species and their organization are virtually identical, it is difficult to exclude a plausible alternative in which full proton transfer is facilitated by adsorption, leading to the formation of hydrogen-bonded adlayers consisting of carboxylate salts of protonated aminotriazine **2a**. To assess this possibility, which has not been noted previously, we calculated the ability of acetic acid to interact with a simplified model, 2-amino-1,3,5-triazine (**4**), to give neutral hydrogen-bonded complex **5** or the salt **6** formed by full proton transfer, both in the gas phase and in the adsorbed state on a graphene model. As described in detail in earlier work and summarized above in the Experimental Section,<sup>13</sup> our calculations were based on the local-density approximation (LDA) of density-functional theory (DFT), and they employed a fixed graphene sheet of defined size and geometry. Dispersive interactions were taken into account by using the PBE functional,<sup>35</sup> in conjunction with semiempirical dispersion corrections (D).<sup>36</sup>



The calculated energies of adsorption, described as being at the PBE+D level, appear in Table 2. In addition, we found that the association of acetic acid with aminotriazine **4** to give hydrogen-bonded complex **5** is exothermic by 23.8 kcal/mol in the gas phase, and salt **6** does not correspond to an energy minimum, in either the gas phase or the adsorbed state. Together, the calculations suggest that the energy of intermolecular association of the adsorbates is similar to their combined energy of adsorption. This confirms that interadsorbate interactions can indeed play a key role in directing molecular organization in 2D, and it provides a theoretical basis for the hypothesis that related 2D and 3D structures can be generated rationally by using flat molecular components that engage in strong directional interactions.

Detailed examination of Table 2 reveals that complex **5** is strongly adsorbed (28.2 kcal/mol), but more weakly (by 8.7 kcal/mol) than the sum of its individual components (36.9 kcal/mol). Hydrogen bonding therefore appears to be weakened slightly by adsorption, as observed in related systems,<sup>13,30</sup> presumably because when NH<sub>2</sub> and COOH groups engage in normal hydrogen bonding they can no longer maintain an optimal orientation with respect to the underlying surface. Nevertheless, our calculations show that the geometries and

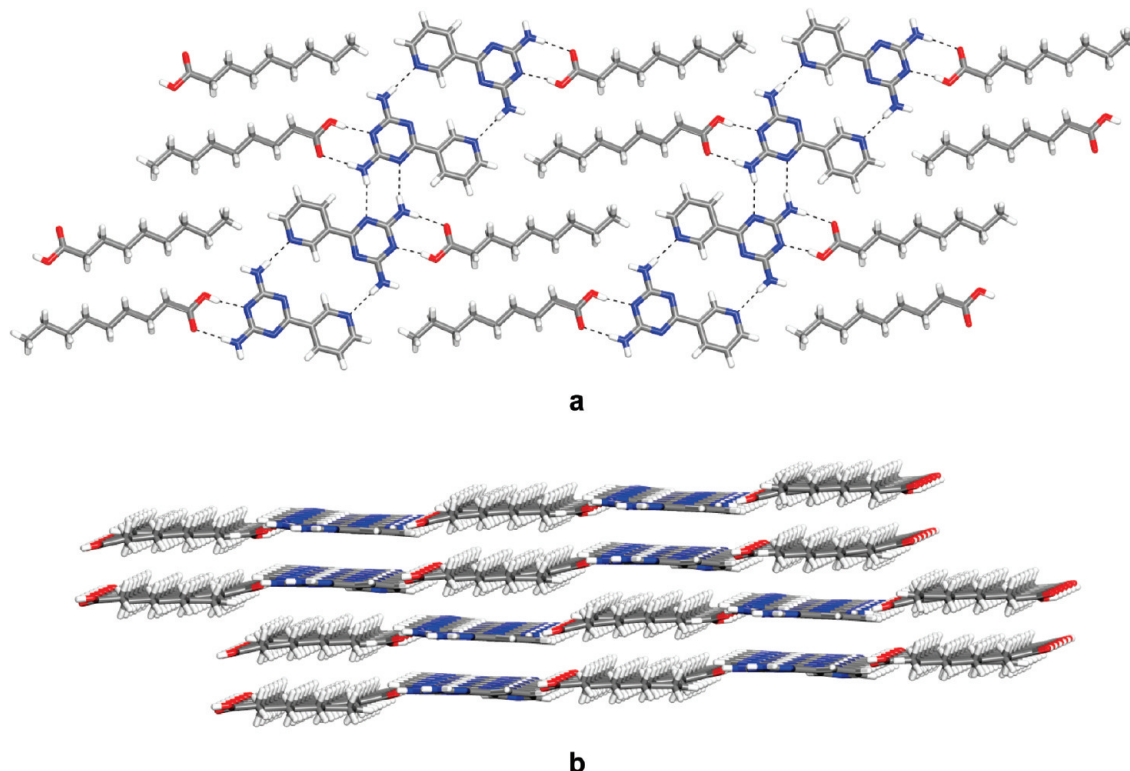


**Figure 4.** Views of the structure of 1:1 cocrystals of 2,4-diamino-6-(3-pyridyl)-1,3,5-triazine (**2b**) with nonanoic acid. (a) View of part of a sheet constructed from hydrogen-bonded tapes. Hydrogen bonds are represented by broken lines, and carbon atoms are shown in gray, hydrogen atoms in white, nitrogen atoms in blue, and oxygen atoms in red. (b) View of four stacked sheets.

atomic charges of hydrogen-bonded complex **5** remain essentially the same in the gas phase and in the adsorbed state on graphene. Together, these results indicate that adsorption does not facilitate full proton transfer, and we conclude that the adsorbed species are the same as those established to be present in 3D structures by XRD.

**3D Cocrystallization of 2,4-Diamino-6-(3-pyridyl)-1,3,5-triazine (2b) with Alkanecarboxylic Acids.** To confirm that the strikingly similar 2D and 3D structures of pyridyl-substituted diaminotriazine **2a** are the result of proper design and not accident, we examined the behavior of isomeric 2,4-diamino-6-(3-pyridyl)-1,3,5-triazine (**2b**). By slow evaporation of a solution of compound **2b** in nonanoic acid at 25 °C, cocrystals of composition **2b**·1 nonanoic acid were obtained. The cocrystals proved to belong to the triclinic space group  $P\bar{1}$ , and other crystallographic data are provided in Table 1. Views of the structure are provided in Figure 4. The particular geometry of compound **2b** allows head-to-tail dimerization by hydrogen bonding of NH<sub>2</sub> groups and the pyridyl nitrogen atom (Figure 4a), and the resulting pairs are linked into chains along the *b* axis by additional hydrogen bonding according to standard synthon I. Further association with nonanoic acid according to synthon II then yields flat tapes analogous to those formed in 2D and 3D by isomeric pyridyl-substituted diaminotriazine **2a**. Packing of the tapes produces sheets with interdigitated alkyl chains (Figure 4a), which stack to generate the 3D structure (Figure 4b).

The crystallographic data show that full proton transfer does not occur to give the corresponding aminotriazinium carboxylate salts.<sup>37–39</sup> The average N–H···N distances within

the hydrogen-bonded pairs (2.958 Å) and synthon I (3.157 Å) have the expected values, and O–H···N and O···H–N distances in synthon II are also normal (2.721 and 2.833 Å, respectively).<sup>19,20</sup> As expected, the average angle formed by the planes of the triazinyl and pyridyl rings is small (3.8°).

**2D Cocrystallization of 2,4-Diamino-6-(3-pyridyl)-1,3,5-triazine (2b) with Alkanecarboxylic Acids.** The preference for hydrogen-bonded sheets in 3D suggests that pyridyl-substituted diaminotriazine **2b** is predisposed to favor a similar molecular organization when coadsorbed with alkanecarboxylic acids on graphite. Addition of a saturated solution of compound **2b** in heptanoic acid to the surface of HOPG yielded an ordered adlayer. Figure 5 shows a representative image, along with a superimposed unit cell and a model of the postulated structure, based on a semiempirical calculation. The patterns of contrast show clear pairing of molecules of compound **2b**, as observed in 3D. Moreover, the unit cell parameters (*a* = 15.4 Å, *b* = 23.2 Å,  $\gamma$  = 60°) provide strong evidence for the formation of chiral tapes that are essentially the same as those observed in 3D (Figure 4a). In 3D, hydrogen-bonded pairs are positioned in the tapes with a periodicity of 13.405(2) Å in 3D, and a similar distance is found in 2D (*a* = 15.4 Å). In addition, adjacent tapes in 3D cocrystals with nonanoic acid are separated by approximately 23.9 Å (as measured along the line defined by the extended alkyl chains), which is consistent with the corresponding distance in 2D cocrystals with heptanoic acid (*b* = 23.2 Å). Furthermore, the angle defined by the tapes and alkyl chains in 3D (approximately 54°) is similar to that found in 2D ( $\gamma$  = 60°). The small differences between 2D and 3D structural

parameters may result in part from efforts to attain optimal registration with the underlying substrate.

Analogous STM images were obtained when pyridyl-substituted diaminotriazine **2b** was coabsorbed on HOPG with

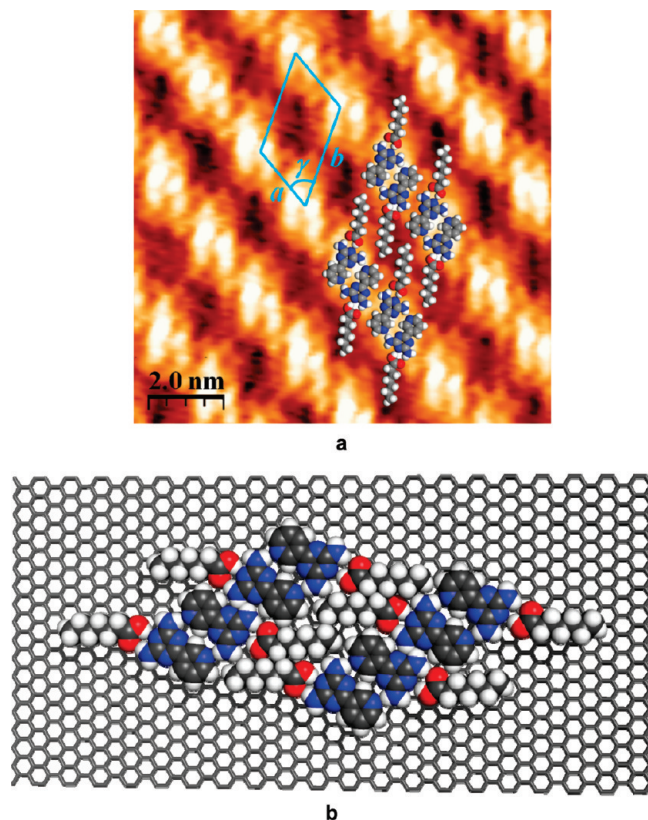


**Figure 5.** (a) STM image of the adsorption of 2,4-diamino-6-(3-pyridyl)-1,3,5-triazine (**2b**) on HOPG (deposition from heptanoic acid, with  $V_{\text{bias}} = -1.50 \text{ V}$  and  $I_{\text{set}} = 0.09 \text{ nA}$ ). Superimposed on the image are a scale bar, the measured unit cell, and approximate molecular models added as visual aids to facilitate interpretation of the pattern of contrasts. (b) Detailed semiempirical model of the proposed 2D structure.

nonanoic acid.<sup>34</sup> As a result, compound **2b** resembles isomer **2a** in its behavior, by cocrystallizing with various alkanecarboxylic acids in 2D and 3D in virtually the same way, as planned. Under all conditions, adjacent domains of adsorbed compounds tended to intersect at angles defined by multiples of  $60^\circ$ , revealing the importance of a particular registration with the underlying surface. This presumably reflects the preference of alkyl chains to align with the symmetry axes of graphite.<sup>34</sup> The strategy of using highly associated adsorbates increases the importance of interadsorbate interactions relative to adsorbate–surface forces, but it does not completely mask the organizing effect of the surface, at least in the present system.

**3D Cocrystallization of 2,4-Diamino-6-(2-pyridyl)-1,3,5-triazine (**2c**) with Alkanecarboxylic Acids.** The notion that certain classes of compounds can be designed to favor similar molecular organization in 2D and 3D was further tested by studying the cocrystallization of isomeric 2,4-diamino-6-(2-pyridyl)-1,3,5-triazine (**2c**) with alkanecarboxylic acids. Slow evaporation of a solution of compound **2c** in octanoic acid at  $25^\circ\text{C}$  yielded cocrystals of composition  $\mathbf{2c} \cdot 1$  octanoic acid. They were found to belong to the triclinic space group  $P\bar{1}$ , and other crystallographic data are summarized in Table 1. A view of the structure is shown in Figure 6. The particular geometry of compound **2c** inhibits the pyridyl nitrogen atom from freely engaging in intermolecular interactions, and individual molecules are linked into chains primarily by normal N–H $\cdots$ N hydrogen bonding (2.917 Å) of the aminotriazinyl groups according to synthon I. The angle formed by the average planes of the triazinyl and pyridyl rings ( $15.9^\circ$ ) is larger than those observed in isomeric pyridyl-substituted diaminotriazines **2a,b**, presumably because an attractive interaryl N $\cdots$ H contact has been replaced by a repulsive N $\cdots$ N contact.

Additional interactions within the chains of compound **2c** include bifurcated N–H $\cdots$ N hydrogen bonds involving the pyridyl nitrogen atom and an NH<sub>2</sub> group (2.998 Å),<sup>40</sup> augmented by a C–H $\cdots$ N interaction (H $\cdots$ N distance = 2.573 Å, C–H $\cdots$ N angle =  $141.8^\circ$ ).<sup>21</sup> Further association of the chains with octanoic acid according to synthon II yields flat tapes closely analogous to those formed in 2D and 3D by isomeric pyridyl-

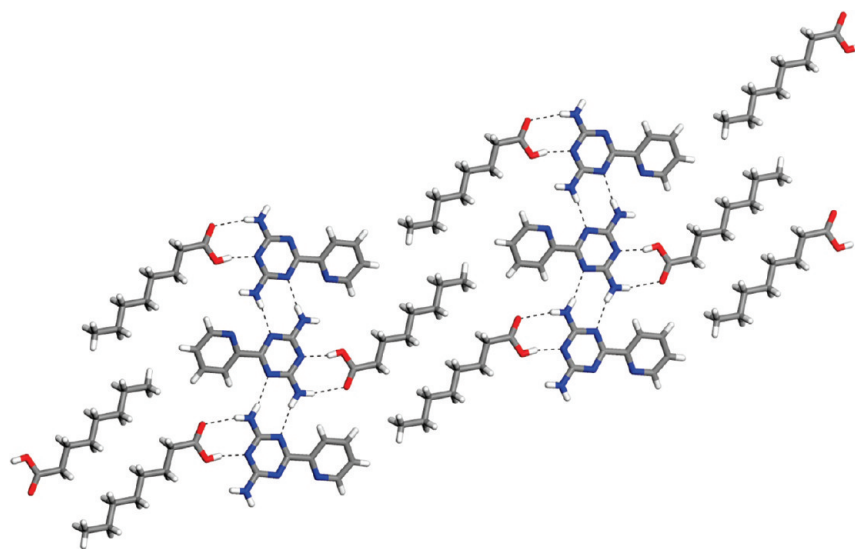


**Figure 6.** View of the structure of 1:1 cocrystals of 6-(2-pyridyl)-2,4-diamino-1,3,5-triazine (**2c**) with octanoic acid, showing part of a sheet constructed from hydrogen-bonded tapes. Principal hydrogen bonds are represented by broken lines, and carbon atoms are shown in gray, hydrogen atoms in white, nitrogen atoms in blue, and oxygen atoms in red.

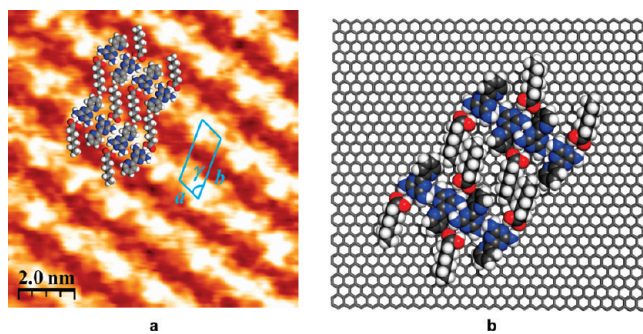


**Figure 7.** (a) STM image of the adsorption of 2,4-diamino-6-(2-pyridyl)-1,3,5-triazine (**2c**) on HOPG (deposition from heptanoic acid, with  $V_{\text{bias}} = -1.50$  V and  $I_{\text{set}} = 0.06$  nA). Superimposed on the image are a scale bar, the measured unit cell, and approximate molecular models added as visual aids to facilitate interpretation of the pattern of contrasts. (b) Detailed semiempirical model of the proposed 2D structure.

substituted diaminotriazine **2b**. O—H $\cdots$ N and O $\cdots$ H—N distances in the tapes are normal (2.622 and 3.080 Å, respectively).<sup>19,20</sup> Packing of the tapes forms sheets with interdigitated alkyl groups (Figure 6), which stack to produce the 3D structure.<sup>34</sup>

As expected, evaporation of solutions of compound **2c** in nonanoic acid yielded 1:1 cocrystals with a closely analogous structure (Table 1).<sup>34</sup> The similarity is clearly revealed by comparing key structural parameters, including intermolecular separation within the tapes, the separation between adjacent tapes (as measured along the line defined by the extended alkyl chains), and the angle defined by the tapes and alkyl chains. These parameters are 6.2 Å, 21.3 Å, and 59.6°, respectively, in cocrystals with octanoic acid, and they are 6.1 Å, 22.2 Å, and 61.6° in cocrystals with nonanoic acid.

**2D Cocrystallization of 2,4-Diamino-6-(2-pyridyl)-1,3,5-triazine (2c) with Alkanecarboxylic Acids.** The strong tendency of pyridyl-substituted diaminotriazine **2c** to cocrystallize with alkanecarboxylic acids to form hydrogen-bonded sheets in 3D suggests that a similar molecular organization will be favored when the components are coadsorbed on graphite. An ordered adlayer was formed on the surface of HOPG when a saturated solution of compound **2c** in heptanoic acid was added. A representative image appears in Figure 7, along with a superimposed unit cell and a model of the proposed structure, calculated by semiempirical methods. The patterns of contrast indicate that compound **2c** forms chiral hydrogen-bonded tapes like those observed in 3D. Moreover, the unit cell parameters ( $a = 7.7$  Å,  $b = 18.2$  Å,  $\gamma = 60^\circ$ ) are consistent with the intratape separations (6.2 and 6.1 Å), intertape distances (21.3 and 22.2 Å), and angles (59.6° and 61.6°) found in 3D cocrystals with octanoic acid and nonanoic acid. Again, pyridyl-substituted diaminotriazine **2c** resembles isomers **2a,b** by cocrystallizing with alkanecarboxylic acids in 2D and 3D in virtually the same way, according to design.

**3D Cocrystallization of 2,4-Diamino-6-[4-(4-pyridyl)phenyl]-1,3,5-triazine (3) with Alkanecarboxylic Acids.** To further probe the predisposition of pyridyl-substituted diaminotriazines to crystallize similarly in 2D and 3D, we examined the behavior of an extended analogue, 2,4-diamino-6-[4-(4-pyridyl)phenyl]-1,3,5-triazine (**3**). By slowly evaporating a solution of compound **3** in heptanoic acid at 25 °C, we obtained cocrystals of composition **3·2** heptanoic acid. They proved to belong to the monoclinic space group  $C2/c$ , and other

**Table 3. Crystallographic Data for Cocrystals of 2,4-Diamino-6-[4-(4-pyridyl)phenyl]-1,3,5-triazine (3) with Alkanecarboxylic Acids (C7 = Heptanoic Acid and C9 = Nonanoic Acid)**

cocrystal	<b>3·2 C7</b>	<b>3·2 C9</b>
formula	$C_{28}H_{40}N_6O_4$	$C_{32}H_{48}N_6O_4$
crystal system	monoclinic	monoclinic
space group	$C2/c$	$C2/c$
$a$ (Å)	50.606(4)	58.554(7)
$b$ (Å)	7.9595(7)	7.9545(10)
$c$ (Å)	14.0826(12)	14.0407(15)
$\alpha$ (°)	90	90
$\beta$ (°)	95.126(4)	102.299(5)
$\gamma$ (°)	90	90
$V$ (Å $^3$ )	5649.8(8)	6389.6(13)
$Z$	8	8
$\rho_{\text{calcd}}$ (g cm $^{-3}$ )	1.234	1.208
$T$ (K)	150	150
$\mu$ (mm $^{-1}$ )	0.679	0.646
$R_1, I > 2\sigma(I)$ (%)	5.97	9.81
$R_{\text{w}}$ , all data (%)	13.32	15.53
$\omega R_2, I > 2\sigma(I)$ (%)	13.67	25.34
$\omega R_2$ , all data (%)	17.03	29.54
measured reflections	37062	48619
independent reflections	5020	4231
observed reflections, $I > 2\sigma(I)$	2591	2484

crystallographic data are summarized in Table 3. Views of the structure appear in Figure 8. Like simpler pyridyl-substituted diaminotriazine **2a**, each molecule of elongated analogue **3** forms hydrogen bonds with two molecules of heptanoic acid according to synthons **II** and **III** to produce ternary aggregates. The observed O—H $\cdots$ N(triazine), O $\cdots$ H—N(triazine), and O—H $\cdots$ N(pyridine) distances in synthons **II** and **III** have normal values (2.608, 3.081, and 2.637 Å, respectively),<sup>19,20</sup> as does the H $\cdots$ O distance (2.705 Å) in the secondary C—H $\cdots$ O interaction of synthon **III**. The carboxyl group is thereby held close to the plane of the pyridyl ring, the alkyl chains adopt an extended conformation, and compound **3** favors a flattened conformation with small interaryl dihedral angles, giving ternary aggregates similar to those observed in 3D structures of cocrystals of analogue **2a** with alkanecarboxylic acids.

In the case of pyridyl-substituted diaminotriazine **2a**, the ternary aggregates are linked to create flat tapes by the formation of in-plane hydrogen bonds and secondary C—H $\cdots$ O interactions. In contrast, the formation of tapes from elongated analogue **3** is dominated by extensive face-to-face aromatic interactions (Figure 8a). Again, packing of the tapes produces sheets; however, molecules of compound **3** are nearly perpendicular to the planes of the sheets (Figure 8b), whereas molecules of simpler analogue **2a** lie within the planes. We attribute this difference to the larger aromatic surface of compound **3**.

Slow evaporation of a solution of compound **3** in nonanoic acid produced cocrystals of composition **3·2** nonanoic acid. These cocrystals were found to have a molecular organization essentially identical to that of cocrystals grown from heptanoic acid (Figure 8), as suggested by comparison of the structural parameters in Table 3.<sup>34</sup> Together, these observations confirm that pyridyl-substituted diaminotriazines **2a–c** and **3** all behave similarly and are properly designed to form closely analogous 3D

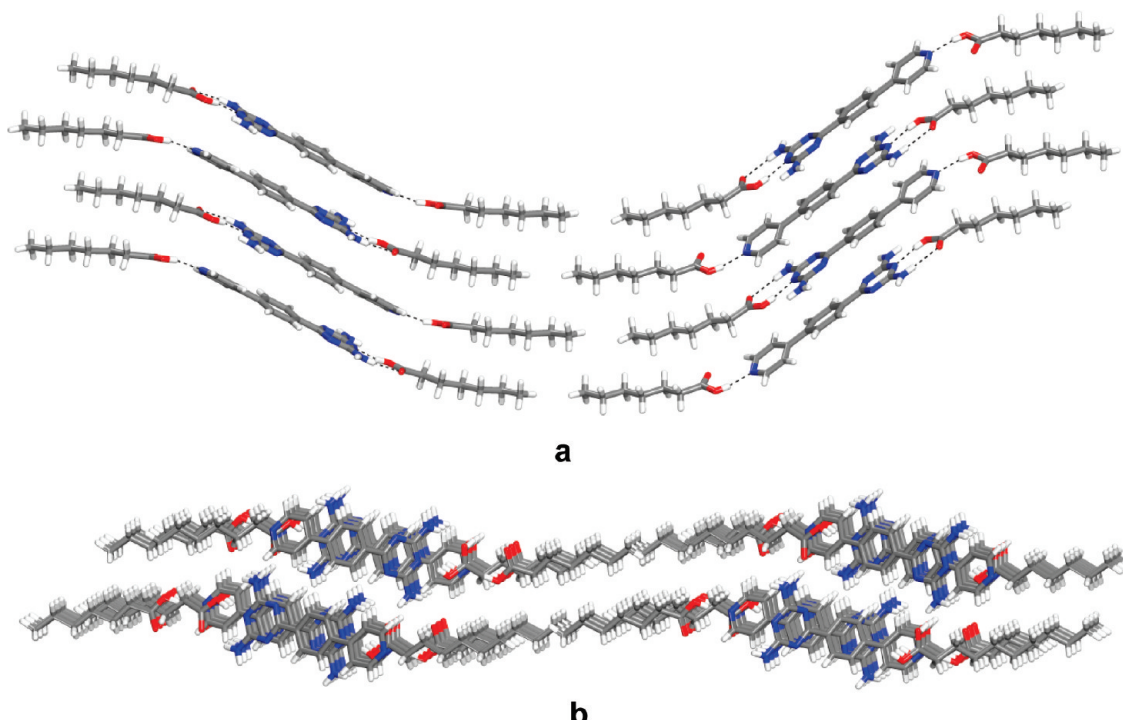


**Figure 8.** Views of the structure of 1:2 cocrystals of 2,4-diamino-6-[4-(4-pyridyl)phenyl]-1,3,5-triazine (**3**) with heptanoic acid. (a) View of part of a sheet constructed from hydrogen-bonded tapes. Hydrogen bonds are represented by broken lines, and carbon atoms are shown in gray, hydrogen atoms in white, nitrogen atoms in blue, and oxygen atoms in red. (b) View of two stacked sheets, showing the nearly perpendicular orientation of molecules of compound **3**.

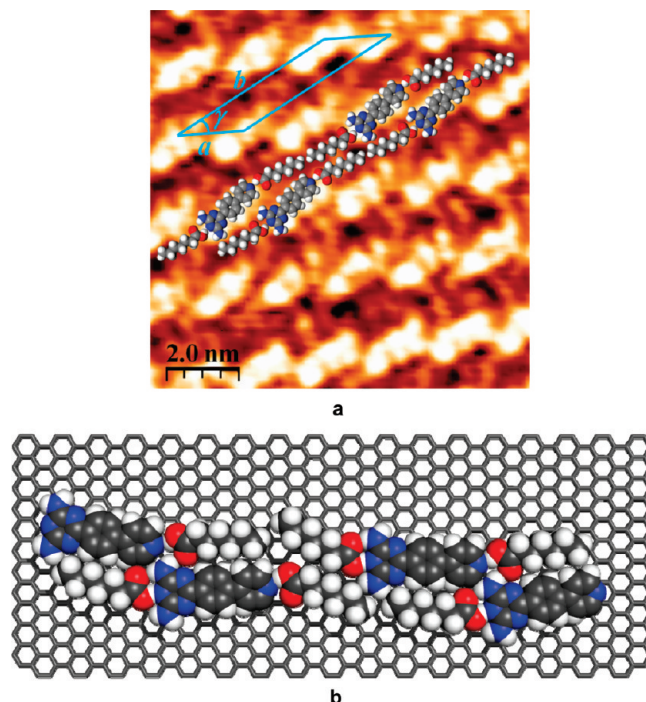


**Figure 9.** (a) STM image of the adsorption of 2,4-diamino-6-[4-(4-pyridyl)phenyl]-1,3,5-triazine (**3**) on HOPG (deposition from heptanoic acid, with  $V_{bias} = -1.16$  V and  $I_{set} = 0.09$  nA). Superimposed on the image are a scale bar, the measured unit cell, and approximate molecular models added as visual aids to facilitate interpretation of the pattern of contrasts. (b) Detailed semiempirical model of the postulated 2D structure.

structures built from sheets incorporating alkanecarboxylic acids. As a result, we were optimistic that compound **3** would resemble relatives **2a–c** by producing analogous 2D cocrystals as well, although we recognized that the perpendicular molecular orientation found in 3D (Figure 8b) would presumably require a degree of alteration to optimize adsorption on graphite.

**2D Cocrystallization of 2,4-Diamino-6-[4-(4-pyridyl)phenyl]-1,3,5-triazine (**3**) with Alkanecarboxylic Acids.** Addition of a saturated solution of compound **3** in heptanoic acid to the surface of HOPG generated an ordered adlayer. Figure 9 shows a representative image, along with a superimposed unit cell and a model of the suggested structure, based on semiempirical calculations. As expected, the patterns of contrast and unit cell parameters ( $a = 16.6$  Å,  $b = 41.2$  Å,  $\gamma = 27^\circ$ ) are consistent with the formation of chiral hydrogen-bonded tapes directly related to those observed in 3D, except that molecules of compound **3** are turned so that they lie in the plane of the adsorbed sheet, parallel to the underlying surface. Again, pyridyl-substituted diaminotriazine **3** resembles analogues **2a–c** by cocrystallizing with alkanecarboxylic acids in 2D and 3D in nearly the same way, as planned.

## CONCLUSIONS

Our results establish that extended series of compounds can be designed to form ordered adlayers and crystalline solids with closely analogous 2D and 3D structures. The observed analogies suggest that the following principles are critical elements of successful design: (1) the molecular components should have a pronounced affinity for the underlying surface to ensure that adsorption takes place; (2) to prevent the surface itself from dictating the organization of adsorbed molecules, which would

typically lead to dissimilar 2D and 3D structures, the cumulative strength of interadsorbate interactions should approach or exceed the energy of adsorption; (3) to maintain structural uniformity in 2D and 3D, the components should engage in strong self-association and be positioned with respect to their neighbors by reliable directional interactions; and (4) these interactions should be directed primarily within a single plane so that the 3D structure can be considered to be built from robust sheets, which are suitable for adsorption without substantial molecular reorganization in 2D.

The behavior of compounds **2a–c** and **3** persuasively illustrates the potential of this approach. In particular, the pyridyl and diaminotriazinyl groups ensure strong adsorption, and the compounds are designed to form hydrogen bonds with alkanecarboxylic acids according to reliable coplanar motifs, thereby ensuring the formation of closely analogous sheets in 2D and 3D. The success of this strategy underscores the rapidly expanding scope of molecular crystal engineering and its potential as a fundamental tool in materials science. We expect our approach to have general value as a source of new molecular materials that favor similar organization in different states, including monolayers, thin films, and bulk solids, allowing their use in applications requiring behavior that depends predictably on dimensions, such as in thin-film devices.

## ■ ASSOCIATED CONTENT

**Supporting Information.** Additional crystallographic details (including thermal atomic displacement ellipsoid plots, powder X-ray diffraction patterns, and tables of structural data in CIF format), supplementary STM images, and analyses of 2D unit cell parameters. This material is available free of charge via the Internet at <http://pubs.acs.org>.

## ■ AUTHOR INFORMATION

### Corresponding Author

\*E-mail: james.d.wuest@umontreal.ca

## ■ ACKNOWLEDGMENT

We are grateful to the Natural Sciences and Engineering Research Council of Canada, the Ministère de l'Éducation du Québec, the Canada Foundation for Innovation, the Canada Research Chairs Program, and Université de Montréal for financial support.

## ■ REFERENCES

- (1) Braga, D. *Chem. Commun.* 2003, 2751–2754. Biradha, K. *CrystEngComm* 2003, 5, 374–384. Hollingsworth, M. D. *Science* 2002, 295, 2410–2413. *Crystal Engineering: From Molecules and Crystals to Materials*; Braga, D., Grepioni, F., Orpen, A. G., Eds.; Kluwer: Dordrecht, Netherlands, 1999. Desiraju, G. R. *Crystal Engineering: The Design of Organic Solids*; Elsevier: Amsterdam, 1989.
- (2) For recent reviews, see: Elemans, J. A. A. W.; De Feyter, S. *Soft Matter* 2009, 5, 721–735. Elemans, J. A. A. W.; Lei, S.; De Feyter, S. *Angew. Chem., Int. Ed.* 2009, 48, 7298–7332. Furukawa, S.; De Feyter, S. *Top. Curr. Chem.* 2009, 287, 87–133. Kühnle, A. *Curr. Opin. Colloid Interface Sci.* 2009, 14, 157–168. Yang, Y.; Wang, C. *Chem. Soc. Rev.* 2009, 38, 2576–2589. Bonifazi, D.; Mohnani, S.; Llanes-Pallas, A. *Chem.—Eur. J.* 2009, 15, 7004–7025. Stepanow, S.; Lin, N.; Barth, J. V. *J. Phys.: Condens. Matter* 2008, 20, 184002. Plass, K. E.; Grzesiak, A. L.; Matzger, A. J. *Acc. Chem. Res.* 2007, 40, 287–293. Barth, J. V. *Annu. Rev. Phys. Chem.* 2007, 58, 375–407. Otero, R.; Rosei, F.; Besenbacher, F. *Annu. Rev. Phys. Chem.* 2006, 57, 497–525. Wan, L.-J. *Acc. Chem. Res.* 2006, 39, 334–342. Barth, J. V.; Costantini, G.; Kern, K. *Nature* 2005, 437, 671–679. De Feyter, S.; De Schryver, F. *J. Phys. Chem. B* 2005, 109, 4290–4302. Smith, R. K.; Lewis, P. A.; Weiss, P. S. *Prog. Surf. Sci.* 2004, 75, 1–68. Moresco, F. *Phys. Rep.* 2004, 399, 175–225. De Feyter, S.; De Schryver, F. *Chem. Soc. Rev.* 2003, 32, 139–150. Hecht, S. *Angew. Chem., Int. Ed.* 2003, 42, 24–26. Giancarlo, L. C.; Flynn, G. W. *Acc. Chem. Res.* 2000, 33, 491–501.
- (3) Gutzler, R.; Sirtl, T.; Dienstmaier, J. F.; Mahata, K.; Heckl, W. M.; Schmittel, M.; Lackinger, M. *J. Am. Chem. Soc.* 2010, 132, 5084–5090. Marie, C.; Silly, F.; Tortech, L.; Müllen, K.; Fichou, D. *ACS Nano* 2010, 4, 1288–1292. Phillips, A. G.; Perdigão, L. M. A.; Beton, P. H.; Champness, N. R. *Chem. Commun.* 2010, 2775–2777. Palma, C.-A.; Bjork, J.; Bonini, M.; Dyer, M. S.; Llanes-Pallas, A.; Bonifazi, D.; Persson, M.; Samori, P. *J. Am. Chem. Soc.* 2009, 131, 13062–13071. Ciesielski, A.; Piot, L.; Samori, P.; Jouaiti, A.; Hosseini, M. W. *Adv. Mater.* 2009, 21, 1131–1136. Zhang, X.; Chen, T.; Chen, Q.; Wang, L.; Wan, L.-J. *Phys. Chem. Chem. Phys.* 2009, 11, 7708–7712. Li, Y.; Ma, Z.; Qi, G.; Yang, Y.; Zeng, Q.; Fan, X.; Wang, C.; Huang, W. *J. Phys. Chem. C* 2008, 112, 8649–8653. Madueno, R.; Räisänen, M. T.; Silien, C.; Buck, M. *Nature* 2008, 454, 618–621. Mamdouh, W.; Kelly, R. E. A.; Dong, M.; Kantorovich, L. N.; Besenbacher, F. *J. Am. Chem. Soc.* 2008, 130, 695–702. Zhou, H.; Dang, H.; Yi, J.-H.; Nanci, A.; Rochefort, A.; Wuest, J. D. *J. Am. Chem. Soc.* 2007, 129, 13774–13775. Ruben, M.; Payer, D.; Landa, A.; Comisso, A.; Gattinoni, C.; Lin, N.; Collin, J.-P.; Sauvage, J.-P.; De Vita, A.; Kern, K. *J. Am. Chem. Soc.* 2006, 128, 15644–15651. Yokoyama, T.; Yokoyama, S.; Kamikado, T.; Okuno, Y.; Mashiko, S. *Nature* 2001, 413, 619–621.
- (4) Dunitz, J. D. *Chem. Commun.* 2003, 545–548. Desiraju, G. R. *Nat. Mater.* 2002, 1, 77–79. Gavezzotti, A. *Acc. Chem. Res.* 1994, 27, 309–314. Maddox, J. *Nature* 1988, 335, 201.
- (5) For initial integrated studies of 2D and 3D crystallization of narrower scope, see: Nath, K. G.; Ivasenko, O.; MacLeod, J. M.; Miwa, J. A.; Wuest, J. D.; Nanci, A.; Perepichka, D. F.; Rosei, F. *J. Phys. Chem. C* 2007, 111, 16996–17007. Dang, H.; Maris, T.; Yi, J.-H.; Rosei, F.; Nanci, A.; Wuest, J. D. *Langmuir* 2007, 23, 11980–11985.
- (6) For reviews of the subject of molecular epitaxy on solid surfaces, see: Witte, G.; Wöll, C. *J. Mater. Res.* 2004, 19, 1889–1916. Hooks, D. E.; Fritz, T.; Ward, M. D. *Adv. Mater.* 2001, 13, 227–241. Forrest, S. R. *Chem. Rev.* 1997, 97, 1793–1896.
- (7) For summaries of these principles, see: Wuest, J. D. *Chem. Commun.* 2005, 5830–5837. Hosseini, M. W. *Acc. Chem. Res.* 2005, 38, 313–323.
- (8) For representative recent examples, see: Meier, C.; Landfester, K.; Ziener, U. *J. Phys. Chem. C* 2009, 113, 1507–1514. Zeng, X.; Wang, L.; Duan, L.; Qiu, Y. *Cryst. Growth Des.* 2008, 8, 1617–1622. Campione, M.; Caprioli, S.; Moret, M.; Sassella, A. *J. Phys. Chem. C* 2007, 111, 12741–12746.
- (9) For recent references, see: Maly, K. E.; Gagnon, E.; Maris, T.; Wuest, J. D. *J. Am. Chem. Soc.* 2007, 129, 4306–4322.
- (10) Binning, G.; Rohrer, H.; Gerber, C.; Weibel, E. *Phys. Rev. Lett.* 1982, 49, 57–61.
- (11) Walch, H.; Maier, A.-K.; Heckl, W. M.; Lackinger, M. *J. Phys. Chem. C* 2009, 113, 1014–1019.
- (12) Zhang, X.; Chen, T.; Chen, Q.; Wang, L.; Wan, L.-J. *Phys. Chem. Chem. Phys.* 2009, 11, 7708–7712.
- (13) Rochefort, A.; Wuest, J. D. *Chem. Commun.* 2010, 2923–2925.
- (14) For a related computational study of the adsorption of melamine (**1**) on Au(111), see: Mura, M.; Martsinovich, N.; Kantorovich, L. *Nanotechnology* 2008, 19, 465704.
- (15) Nangia, A.; Desiraju, G. R. *Top. Curr. Chem.* 1998, 198, 57–95. Desiraju, G. R. *Angew. Chem., Int. Ed.* 1995, 34, 2311–2327.
- (16) Díaz-Ortíz, Á.; Elguero, J.; Foces-Foces, C.; de la Hoz, A.; Moreno, A.; del Carmen Mateo, M.; Sánchez-Migallón, A.; Valiente, G. *New J. Chem.* 2004, 28, 952–958.
- (17) Ma, D.-L.; Che, C.-M. *Chem.—Eur. J.* 2003, 9, 6133–6144.

- (18) Chan, C.-W.; Mingos, D. M. P.; White, A. J. P.; Williams, D. J. *Polyhedron* **1996**, *15*, 1753–1767.
- (19) Pedireddi, V. R.; Chatterjee, S.; Ranganathan, A.; Rao, C. N. R. *Tetrahedron* **1998**, *54*, 9457–9474. Etter, M. C.; Adsmond, D. A. *Chem. Commun.* **1990**, 589–591. Garcia-Tellado, F.; Goswami, S.; Chang, S.-K.; Geib, S. J.; Hamilton, A. D. *J. Am. Chem. Soc.* **1990**, *112*, 7393–7394.
- (20) For recent references, see: Singh, D.; Bhattacharyya, P. K.; Baruah, J. B. *Cryst. Growth Des.* **2010**, *10*, 348–356. Shattock, T. R.; Arora, K. K.; Vishweshwar, P.; Zaworotko, M. J. *Cryst. Growth Des.* **2008**, *8*, 4533–4545. Babu, N. J.; Nangia, A. *Cryst. Growth Des.* **2006**, *6*, 1995–1999. Aakeröy, C. B.; Desper, J.; Urbina, J. F. *CrystEngComm* **2005**, *7*, 193–201. Dale, S. H.; Elsegood, M. R. J.; Hemmings, M.; Wilkinson, A. L. *CrystEngComm* **2004**, *6*, 207–214.
- (21) Desiraju, G. R.; Steiner, T. *The Weak Hydrogen Bond in Structural Chemistry and Biology*; Oxford University Press: Oxford, U. K., 1999.
- (22) For a review of C–H···O interactions, see: Desiraju, G. R. *Chem. Commun.* **2005**, 2995–3001.
- (23) For recent examples and further discussion, see: Phillips, T. K.; Bhinde, T.; Clarke, S. M.; Lee, S. Y.; Mali, K. S.; De Feyter, S. *J. Phys. Chem. C* **2010**, *114*, 6027–6034. Hai, N. T. M.; Van der Auweraer, M.; Müllen, K.; De Feyter, S. *J. Phys. Chem. C* **2009**, *113*, 11567–11574. Plass, K. E.; Kim, K.; Matzger, A. J. *J. Am. Chem. Soc.* **2004**, *126*, 9042–9053.
- (24) Baibulova, M. S.; Akkulova, Z. G.; Afanas'eva, T. A. *Izv. Akad. Nauk Kaz. SSR, Ser. Khim.* **1989**, 40–42.
- (25) Case, F. H.; Koft, E. *J. Am. Chem. Soc.* **1959**, *81*, 905–906.
- (26) For previous syntheses, see: Cho, S.-D.; Kim, H.-K.; Yim, H.-s.; Kim, M.-R.; Lee, J.-K.; Kim, J.-J.; Yoon, Y.-J. *Tetrahedron* **2007**, *63*, 1345–1352. Evans, O. R.; Lin, W. *Chem. Mater.* **2001**, *13*, 2705–2712. Le Gall, E.; Gosmini, C.; Nédélec, J.-Y.; Périchon, J. *Tetrahedron* **2001**, *57*, 1923–1927. Lin, S.-T.; Yang, F.-M.; Liang, D.; Shiao, M.-J. *J. Chin. Chem. Soc.* **1997**, *44*, 527–533.
- (27) Simons, J. K.; Saxton, M. R. *Organic Syntheses*; Wiley: New York, 1963; Collect. Vol. IV, p 78.
- (28) Horcas, I.; Fernández, R.; Gómez-Rodríguez, J. M.; Colchero, J.; Gómez-Herrero, J.; Baro, A. M. *Rev. Sci. Instrum.* **2007**, *78*, 01375.
- (29) Rocha, G. B.; Freire, R. O.; Simas, A. M.; Stewart, J. J. P. *J. Comput. Chem.* **2006**, *27*, 1101–1111.
- (30) Rochefort, A.; Wuest, J. D. *Langmuir* **2009**, *25*, 210–215.
- (31) For recent related calculations of physisorption on graphene, see: Henwood, D.; Carey, J. D. *Mol. Simul.* **2008**, *34*, 1019–1023. Zhechkov, L.; Heine, T.; Seifert, G. *Int. J. Quantum Chem.* **2006**, *106*, 1375–1382.
- (32) MOPAC2009 Version 9.351M (James J. P. Stewart, Stewart Computational Chemistry; [HTTP://OpenMOPAC.net](http://OpenMOPAC.net)).
- (33) Sheldrick, G. M. *Acta Crystallogr.* **2008**, *A64*, 112–122.
- (34) See the Supporting Information for details.
- (35) Perdew, J. P.; Burke, K.; Ernzerhof, M. *Phys. Rev. Lett.* **1996**, *77*, 3865–3868.
- (36) Grimme, S. *J. Comput. Chem.* **2006**, *27*, 1787–1799.
- (37) The small difference between the  $pK_a$  values of alkanecarboxylic acids and those of the conjugate acids of pyridine or amino-triazines such as melamine ( $pK_a$  5)<sup>38</sup> provides little driving force for proton transfer.<sup>39</sup>
- (38) Jang, Y. H.; Hwang, S.; Chang, S. B.; Ku, J.; Chung, D. S. *J. Phys. Chem. A* **2009**, *113*, 13036–13040.
- (39) For discussion, see: He, G.; Chow, P. S.; Tan, R. B. H. *Cryst. Growth. Des.* **2009**, *9*, 4529–4532. Mohamed, S.; Tocher, D. A.; Vickers, M.; Karamertzanis, P. G.; Price, S. L. *Cryst. Growth. Des.* **2009**, *9*, 2881–2889. Childs, S. L.; Stahly, G. P.; Park, A. *Mol. Pharmaceutics* **2007**, *4*, 323–338. Bhogala, B. R.; Basavojju, S.; Nangia, A. *CrystEngComm* **2005**, *7*, 551–562.
- (40) For examples of related bifurcated hydrogen bonds, see: Aghabozorg, H.; Gharamaleki, J. A.; Olmstead, M. M.; Derikvand, Z.; Hooshmand, S. *Acta Crystallogr.* **2009**, *E65*, m186–m187. Šmejkal, T.; Breit, B. *Angew. Chem., Int. Ed.* **2008**, *47*, 311–315. Preston, A. J.; Gallucci, J. C.; Parquette, J. R. *Chem. Commun.* **2005**, 3280–3282. Bell, T. W.; Khasanov, A. B.; Drew, M. G. B. *J. Am. Chem. Soc.* **2002**, *124*, 14092–14103. Bell, T. W.; Khasanov, A. B.; Drew, M. G. B.; Filikov, A.; James, T. L. *Angew. Chem., Int. Ed.* **1999**, *38*, 2543–2547.